Droplet jump-off force on a superhydrophobic surface

Juan Li [1,2] Alexander Oron [2] and Youhua Jiang [1,2,3,*]

[1]*Department of Mechanical Engineering, Guangdong Technion–Israel Institute of Technology, Shantou, Guangdong 515063, China*

[2]*Faculty of Mechanical Engineering, Technion–Israel Institute of Technology, Haifa 3200003, Israel*

[3]*Guangdong Provincial Key Laboratory of Materials and Technologies for Energy Conversion, Guangdong Technion–Israel Institute of Technology, Shantou, Guangdong 515063, China*

(Received 4 August 2023; accepted 30 October 2023; published 17 November 2023)

Droplet impact onto solid substrates is not only an interesting natural phenomenon, but also has applications in various fields. Recent studies in the literature reported that following the first peak of the force exerted on a superhydrophobic substrate by the droplet at the moment of impact, the droplet retraction and jump-off led to the emergence of a second peak of this force, which scales with the inertia-dominated impact force. In this paper, we have found this result to fail in the case of droplets with a broadly varying viscosity. New scaling models based on the observation of flow focusing are proposed to express the relevant timescale and the magnitude of the second force peak.

DOI: 10.1103/PhysRevFluids.8.113601

I. INTRODUCTION

An ancient Chinese proverb near 105 AD says: "drops of water wear holes in stone." Although this proverb was intended to highlight the importance of determination and persistence, it suggests that the impact of a liquid droplet onto a solid substrate is one of the most pervasive natural phenomena. In addition, droplet impact on a solid substrate is important to various droplet-related applications, such as ink-jet printing, spray cooling, coating, fog collection, respiratory disease control, and others [1–6]. Droplet impact on a solid surface serves as a basis for the investigation of the following dynamics: the maximal spreading diameter, the droplet-substrate contact time, the energy dissipation from impact to rebound, and the force imparted to the substrate by the impact [7–15].

A newly reported phenomenon shows that in addition to the first force (impact force) exerted on the substrate, the droplet retraction and jump-off on a *superhydrophobic* substrate leads to the emergence of a second force imparted to the substrate referred to as the jump-off force hereafter [9,16,17]. The jump-off force results primarily from the abrupt change in the fluid momentum from that in the direction parallel to the substrate to that perpendicular to it, which is referred to as flow focusing. As shown in Fig. 1(a), a hole with a diameter around one-third of the initial droplet diameter is observed on a superhydrophobized plaster slab after releasing water droplets at a height of 5 cm to impact onto the slab every 8 s for 4 h. In contrast to the finding [18] that the observed erosion is due to the inertia-dominated droplet impact (the first force) whose size could thus be close to the initial droplet diameter, we argue that the droplet jump-off (the second) force plays a dominant role instead. This observation is in line with droplet penetration through a superhydrophobic mesh, where the droplet penetrates the mesh more easily in the retraction phase than in that of spreading [19]. This suggests that the emergence of the droplet jump-off force is not only fundamentally

*To whom correspondence should be addressed: youhua.jiang@gtiit.edu.cn

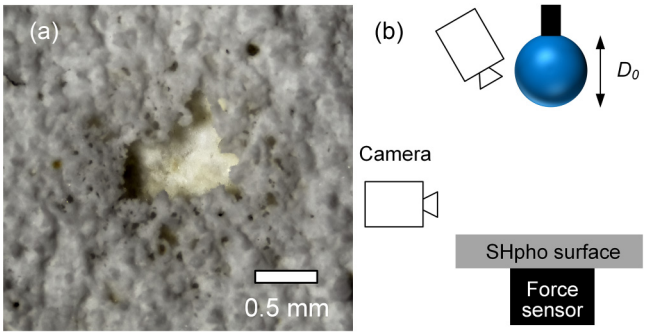

FIG. 1. (a) Surface morphology of a superhydrophobized plaster slab after being collided by 6.6-μl water droplets released at a height of 5 cm above the substrate every 8 s for 4 h, where a hole with an average diameter of ∼0.8 mm is observed. (b) Schematics of the experimental setup: a droplet with a diameter of D_0 impacts onto a superhydrophobic (SHpho) surface, which is placed on top of the force sensor.

intriguing, but it is also practically important in the applications such as erosion protection [20–23]. Therefore, we restrict this paper to the investigation of the droplet jump-off force.

It was shown [9,16] that the jump-off force scales with the dynamic pressure ρV_0^2 multiplied by the droplet base area D_0^2 in the range of $30 < \mathrm{We} < 100$, where ρ, V_0, D_0, and γ_{LV} represent the droplet density, its impact speed, its diameter, and the liquid-vapor interfacial tension, respectively, and $\mathrm{We} = \rho V_0^2 D_0/\gamma_{\mathrm{LV}}$ is the Weber number. In the range of $\mathrm{We} < 30$, the second force arises from a singular jet due to the burst of the air cavity [24–26] and, hence, is outside the scope of this paper. For very large We, droplets exhibit various complexities due to droplet rim instability and splashing [2,27] and, therefore, are also beyond the scope of the present paper.

As compared with earlier studies [9,16], we find the scaling law deduced there to be invalid for droplets with varying viscosity in a way that the power of V_0 in the magnitude of the jump-off force decreases with an increase in viscosity. Therefore, it is the purpose of this paper to propose a scaling model uniform for the timescale based on the flow focusing that occurs on this timescale, and for the magnitude of the jump-off force for droplets of different viscosities in the range of Weber numbers $30 < \mathrm{We} < 170$.

II. EXPERIMENTS AND METHODS

In the experiments, droplets with the volume of 4.8–6.6 μl equivalent to $D_0 = 2.2 \pm 0.15$ mm were generated by a syringe pump and released at different heights to impact onto a superhydrophobic aluminum plate (advancing and receding contact angles of $160^\circ \pm 5^\circ$ and $155^\circ \pm 5^\circ$, respectively), placed on top of the force sensor (9215A; Kistler, Winterthur, Switzerland). Analog force data was amplified by a charge amplifier (5018A; Kistler, Winterthur, Switzerland) and sampled by a sampling system (SIRIUSm; DeweSoft, Slovenia) at a frequency of 2×10^5 Hz. Two high-speed cameras (Nova S16; Photron, Japan) were triggered simultaneously to capture the top and side views of the droplet evolution at the speed of 10 000 frames per second, as schematically shown in Fig. 1(b). Droplets with different viscosities 1 mPa s $< \mu <$ 37 mPa s, slightly varying densities ρ, and liquid-vapor interfacial tension γ_{LV} created by manipulating the water-glycerol mixture ratios, were tested and the average of at least five reproducible data are reported in what follows. Specifically, the viscosity of de-ionized (DI) water, DI water containing 45, 60, and 75 wt% of glycerol is 1.0, 4.5, 10.0, and 36.7 mPa s, respectively. Note that droplets with a higher viscosity were not studied due to technical difficulties, such as a very weak jump-off force and its very slow variation with time.

Detailed experimental procedures, including details of the preparations of superhydrophobic aluminum plates, superhydrophobization of plaster slabs, fabrication of ridges, and experimental

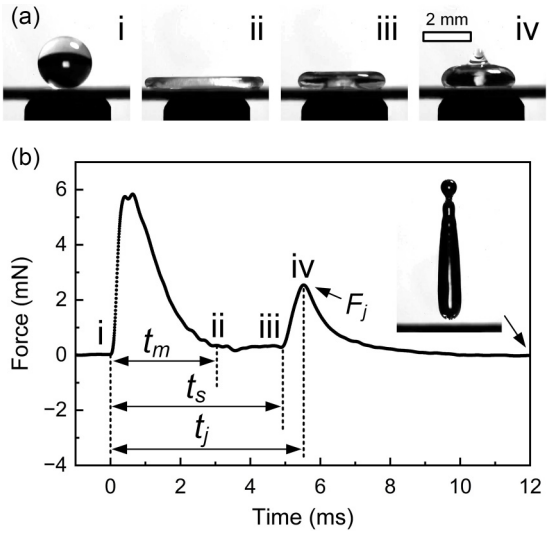

FIG. 2. (a) Shape profiles of a 6.6-μl water droplet released at a height of 7 cm after impacting onto a superhydrophobic substrate: (i) the droplet-substrate initial contact takes place at $t = t_0$; (ii) the maximal spreading at $t = t_m$; (iii) the moment when the second (jump-off) force starts to increase abruptly at t_s, and (iv) the moment when the second (jump-off) force reaches its peak F_j at $t = t_j$. (b) Temporal variation of the force exerted onto the substrate.

parameters (Table S1) can be found in the Supplemental Material [28]. Briefly, superhydrophobic aluminum plates were prepared using a process known as boehmitization to produce surface nanostructures [29] followed by hydrophobization via chemical vapor deposition of 1H,1H,2H,2H-perfluorodecyltrichlorosilane. Superhydrophobic plaster slabs were prepared by spray-coating hydrophobic SiO_2 nanoparticles onto commercially available plaster slabs [5]. The ridged substrates were prepared by selectively removing the surface materials of aluminum plates and plaster slabs using a laser etcher.

III. RESULTS AND DISCUSSION

A. Experimental observations

The evolution of a water droplet released at a height of 7 cm upon its impact onto the substrate and the corresponding time variation of the force exerted on the substrate are presented in Figs. 2(a) and 2(b), respectively (see also Video S1 in the Supplemental Material [28]). Since the object of interest is the second force (jump-off force, F_j), starting from the force at $t = 0$ (the moment of the initial contact between the droplet and the substrate), we only label the stages of the droplet evolution in association with F_j including the time of the maximal spreading, which is the moment right before the droplet retraction, $t = t_m$, the moment when the second (jump-off) force starts to suddenly increase, $t = t_s$, and the moment when the jump-off force reaches its peak, $t = t_j$. Typically, t_s locates at the moment when the force magnitude reaches $20\% \pm 5\%$ of F_j and at this moment, the force transits from oscillation regime to a monotonic rise. The above definition of these times yields two important timescales related to the flow focusing, which may become important for the determination of the droplet jump-off force: $t_1 = t_j - t_m$ and $t_2 = t_j - t_s$. The former is associated with the entire period from the onset of retraction to flow focusing, whereas the latter disregards the early period of retraction, typically 60%–80% of t_1, as there is a negligible vertical force imparted to the substrate due to the lack of variation in the vertical flow speed. Here, t_2 is referred to hereafter

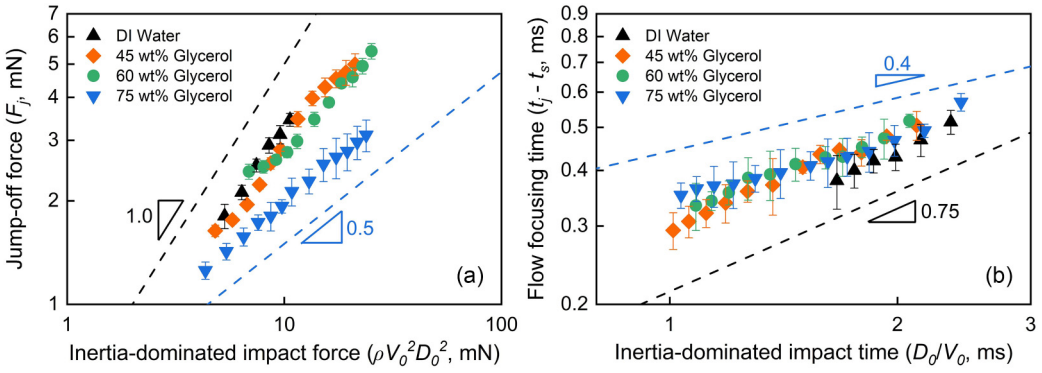

FIG. 3. (a) Variation of the measured jump-off force F_j with the inertia-dominated impact force $\rho V_0^2 D_0^2$ and (b) variation of the measured flow focusing time $t_2 = t_j - t_s$ with the inertia-dominated timescale D_0/V_0. The viscosity of DI water; DI water containing 45, 60, and 75 wt% of glycerol is 1.0, 4.5, 10.0, and 36.7 mPa s, respectively.

as the flow focusing time and is believed to be directly relevant to F_j, since it corresponds to the sudden increase in the force magnitude, and, therefore, t_1 will not be further considered.

It should be noted that the situation when F_j is scaled with $\rho V_0^2 D_0^2$ stems from the momentum flux balance in the vertical direction with inertia as the dominant factor, that is, $F_j \sim \rho D_0^3 V_0/(D_0/V_0)$. Therefore, we plot the measured jump-off force F_j versus the inertia-dominated impact force $\rho V_0^2 D_0^2$ and the measured flow focusing time t_2 with the inertia-dominated timescale D_0/V_0 in Figs. 3(a) and 3(b), respectively. In remarkable contrast to the results presented in [9,16], Fig. 3(a) shows that only in the case of water droplets, the jump-off force scales linearly with $\rho V_0^2 D_0^2$. The jump-off force in the case of droplets with higher viscosities do not collapse on the same curve, nor even agree with the above scaling. For example, droplets containing 75 wt% glycerol exhibit a scaling with $\rho V_0^2 D_0^2$ to the power of ~0.5. Similarly, Fig. 3(b) shows that the flow focusing time does not scale linearly with D_0/V_0 and a higher viscosity causes a more pronounced deviation from the linear relationship. Moreover, we have found that the flow focusing time does not scale with the velocity-independent inertia-capillary time (contact time between the droplet and the substrate) $\sqrt{\rho D_0^3/\gamma_{LV}}$ [7] nor with the visco-capillary time $D_0\mu/\gamma_{LV}$ [30]. These disparities suggest that the jump-off force may involve a more intricate correlation with capillarity, inertia, and viscosity, and this will be elaborated in the following.

B. Model of flow focusing time

We use the momentum balance in the vertical direction for the scaling argument, but the change in the vertical speed should not be V_0 due to dissipation; in other words, the droplet rebounds with a speed lower than V_0 [31]. The flow focusing timescale should not be D_0/V_0 because the droplet retraction is governed by capillarity. Panels (ii) and (iii) of Fig. 2(a) show that upon the impact of the droplet on the substrate, the droplet flattens out and assumes a pancakelike shape. Hence, to analyze the flow focusing stage of the droplet evolution, we consider a pancake (cylindrical) droplet retracting with the speed of V_{re}, a maximal spreading diameter of D_{max}, and a thickness of h as a model for scaling analysis, as schematically shown in Fig. 4(a). The droplet retraction causes a small cylindrical domain around the center of the puddle to be squeezed and, as a result, to produce a vertical flow upwards with a speed of V_{up} and an effective cross-section area of A_{eff}. All these values are related via $\pi D_{max} h V_{re} \approx A_{eff} V_{up}$, that is, the flow rate of the radially receding flow is fully transformed to that of the upward flow. The volume conservation $D_{max}^2 h \sim D_0^3$ and the widely accepted correlation $D_{max} \sim D_0 \mathrm{We}^{1/4}$ [see Fig. 4(b) [8] yield an expression for the thickness of the

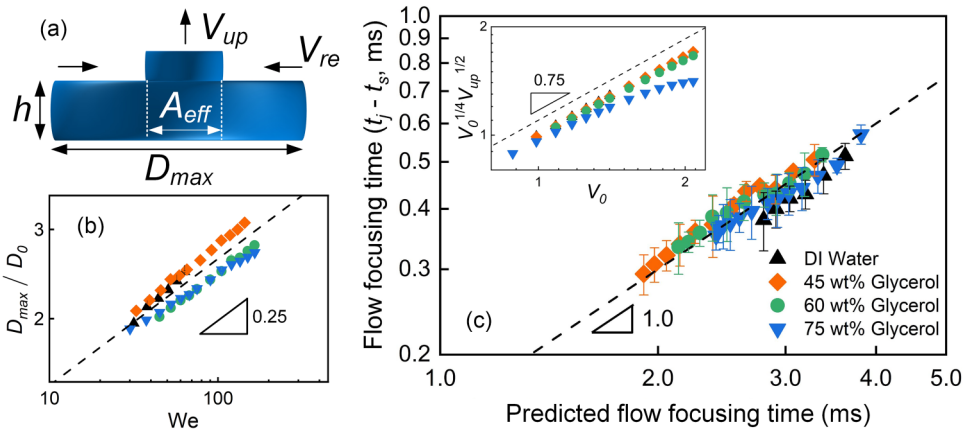

FIG. 4. (a) Schematic of a simplified cylindrical puddle with a maximal spreading diameter of $D_{\max}$, a thickness of h, and a retraction speed of $V_{\rm re}$, which causes an upward flow with a speed of $V_{\rm up}$ and an effective area of $A_{\rm eff}$. (b) The measured maximal spreading diameter normalized by the droplet initial diameter $D_{\max}/D_0$ versus the Weber number, We, where the dashed line represents the scaling of $D_{\max}/D_0 \sim {\rm We}^{1/4}$. (c) The measured flow focusing time t_2 versus the predicted flow focusing time given by Eq. (1) with a fitting coefficient $c = 0.02$ in Eq. (2). The dashed curve represents a straight line as a guide for the eyes. The inset shows the variation of $V_0^{1/4}V_{\rm up}^{1/2}$ with V_0, whose scaling with V_0 varies for different droplet viscosities.

cylindrical droplet $h \sim \sqrt{\gamma_{\rm LV} D_0/\rho V_0^2}$ [8,19]. The droplet retraction rate and the droplet-substrate contact time were reported to be independent of the impact speed [7,32]. Therefore, using the inertia-capillary speed, which is given by the ratio between the droplet diameter D_0 and the impact speed-independent inertia-capillary time $\sqrt{\rho D_0^3/\gamma_{\rm LV}}$, thus expressing the droplet retraction speed as $V_{\rm re} \sim \sqrt{\gamma_{\rm LV}/\rho D_0}$, the effective area $A_{\rm eff}$ can be now defined as $A_{\rm eff} \sim D_0^{5/4}\gamma_{\rm LV}^{3/4}/(\rho^{3/4}V_0^{1/2}V_{\rm up})$. It should be noted that the retraction speed can be alternatively approximated by the Taylor-Culick speed $V_{\rm re} \sim \sqrt{\gamma_{\rm LV}/\rho h}$ [27,32,33], leading to a negligible difference in results. Nevertheless, the jump-off force is exerted when the droplet is squeezed and the radial flow is redirected to the upward flow (from iii to iv in Fig. 2), suggesting that the retraction speed is decreasing. As such, we choose the inertia-capillary speed for the sake of simplicity, rather than the Taylor-Culick speed, which captures a constant or the maximal retraction speed of the droplet. We argue that the flow focusing occurs within the effective area with a length scale of $\sqrt{A_{\rm eff}}$ and the liquid is squeezed radially and changes its direction to the vertical one within the core of $A_{\rm eff}$. Therefore, the flow focusing time is estimated as

$$t_2 \sim \frac{\sqrt{A_{\rm eff}}}{V_{\rm re}} \sim \frac{D_0^{9/8}\rho^{1/8}}{\gamma_{\rm LV}^{1/8}V_0^{1/4}V_{\rm up}^{1/2}}. \tag{1}$$

Assuming the kinetic energy of the puddle is dissipated due to the liquid viscosity in the process of spreading and retraction, we find that a decrease in the droplet speed from V_0 at the impact to $V_{\rm up}$ at the jump, and the value of $V_{\rm up}$ can be approximated as

$$V_{\rm up} \sim \sqrt{V_0^2 - \frac{2E_{\rm vis}}{m}c}, \tag{2}$$

where $E_{\rm vis}$ is the viscous dissipation energy, $m = \pi D_0^3\rho/6$ is the droplet mass, and c is a fitting coefficient expressing uncertainties and simplifications in the scaling arguments for $E_{\rm vis}$, which is believed to be a constant in the tested range of experimental parameters. Specifically, the energy loss

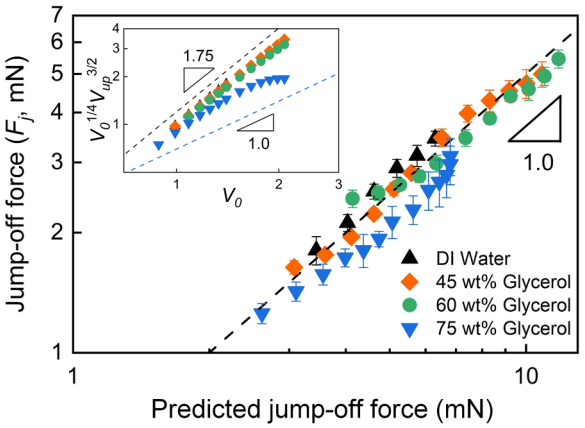

FIG. 5. Variation of the measured jump-off force F_j with the predicted jump-off force determined via Eq. (4) with a fitting coefficient $c = 0.02$. The dashed curve represents a straight line as a guide for the eyes. The inset shows the variation of $V_0^{1/4}V_{up}^{3/2}$ with V_0.

associated with contact angle hysteresis is ignored due to the extremely low contact angle hysteresis on superhydrophobic surfaces. Here, we assume that the entire pancakelike droplet contributes to the viscous dissipation, since the boundary layer thickness $\sim\sqrt{\mu D_0/\rho V_0}$ exceeds the droplet thickness h for viscous liquids. Considering the effective volume that contributes to the viscous dissipation $D_{max}^2 h \sim D_0^3$, the viscous dissipation per unit volume and unit time is $\mu(\partial u/\partial z)^2 \sim \mu(V_0/h)^2$, and given that the droplet-substrate contact time is $\sim\sqrt{\rho D_0^3/\gamma_{LV}}$, the viscous dissipation E_{vis} is obtained as

$$E_{vis} \sim \mu V_0 D_0^2 \mathrm{We}^{3/2}. \tag{3}$$

As follows from Eq. (3), the scaling of E_{vis} with V_0^4 indicates that a larger droplet impact speed leads to a more significant viscous dissipation. Taking into consideration Eqs. (2) and (3), we display in Fig. 4(c) the *measured* flow focusing time t_2 versus the predicted one based on Eq. (1). As compared with Fig. 3(b), where the data for droplets with different viscosities do not collapse on the same curve, all data now collapse on a master straight line with the fitting coefficient $c = 0.02$. This takes place because V_{up} scales linearly with V_0 for low-viscosity droplets, since E_{vis} is small in Eq. (2) and, hence the flow focusing time follows $t_2 \sim V_0^{-1/4}V_{up}^{-1/2} \sim V_0^{-3/4}$, which agrees with the measurements for water droplets in Fig. 3(b). With an increase in viscosity, the power of scaling of V_{up} with V_0 becomes less than 1, and therefore, the flow focusing time t_2 scales with V_0 with a power higher than $-3/4$, which is confirmed for droplets containing 75 wt% of glycerol in Fig. 3(b). The above arguments are demonstrated in the inset of Fig. 4(c) by displaying the variation of $V_0^{1/4}V_{up}^{1/2}$ with V_0.

C. Model for jump-off force

Taking into account the liquid mass involved in flow focusing $\sim\rho D_0^3$, the change in the vertical speed V_{up}, and the flow focusing time t_2, the jump-off force F_j imposed by the droplet onto the substrate is given by

$$F_j \sim \frac{\rho D_0^3 V_{up}}{t_2} \sim \rho^{7/8} D_0^{15/8} \gamma_{LV}^{1/8} V_0^{1/4} V_{up}^{3/2}. \tag{4}$$

Figure 5 now presents the variation of the measured jump-off force F_j with its theoretical values based on Eq. (4). As compared with Fig. 3(a), where the measured results for droplets with different

viscosities are scattered and do not even share the same scaling with V_0, all measured results for the droplets with varying viscosities now collapse onto a straight master line with the fitting coefficient of $c = 0.02$.

As discussed above, in the case of low-viscosity droplets, one has $V_0^{1/4}V_{up}^{3/2} \sim V_0^{7/4}$. Since $V_0^{7/4}$ is close to V_0^2, $D_0^{15/8}$ is close to D_0^2, $\rho^{7/8}$ is close to ρ, and $\gamma_{LV}^{1/8}$ is close to $\gamma_{LV}^0 \approx 1$, our model supports the results of the previous investigations for *water* droplets that the jump-off force scales with the inertia-dominated impact force $\rho V_0^2 D_0^2$ [9,16]. With an increase in viscosity, the value $V_0^{1/4}V_{up}^{3/2}$ scales with V_0 with the power less than 7/4 as seen in the inset in Fig. 5. This explains the observations presented in Fig. 3(a) that the scaling power of $\rho V_0^2 D_0^2$ decreases from 1 for water droplets to around 0.5 for droplets with the highest viscosity of 75 wt% of glycerol. We note that since V_{up} is an intermediate variable, the flow focusing time given in Eq. (1) and the jump-off force given in Eq. (4) may be fully expressed via V_0 by substituting V_{up} as a function of V_0 based on the data represented in the inset to Fig. 4(c).

In addition to the flow focusing time and the droplet jump-off force that have been experimentally measured in this investigation, we now discuss the jump-off pressure P_j imparted by a recoiling droplet to the substrate using experimental results in literature. Ryu *et al.* [19] measured P_j on superhydrophobic meshes by adjusting the critical impact speed of a water droplet that leads to liquid penetration, where P_j is the resisting capillary pressure of a pore with a known size. By systematically varying the pore geometry, Ryu *et al.* [19] found that the jump-off pressure is $P_j \sim \rho^{3/2} D_0^{1/2} V_0^3 \gamma_{LV}^{-1/2}$. Based on our approach, the pressure can be estimated using the jump-off force F_j divided by the effective area A_{eff}, as

$$P_j \sim \frac{F_j}{A_{eff}} \sim \frac{\rho^{13/8} D_0^{5/8} V_0^{3/4} V_{up}^{5/2}}{\gamma_{LV}^{5/8}}. \tag{5}$$

For water droplets, $V_0^{3/4}V_{up}^{5/2}$ can be replaced by $V_0^{13/4}$. Since $\rho^{13/8}$ is close to $\rho^{3/2}$, $D_0^{5/8}$ is close to $D_0^{1/2}$, $V_0^{13/4}$ is close to V_0^3, and $\gamma_{LV}^{5/8}$ is close to $\gamma_{LV}^{1/2}$, the predicted pressure in Eq. (5) roughly equals to $\sim \rho^{3/2} D_0^{1/2} V_0^3 \gamma_{LV}^{-1/2}$, which agrees with the reported experimental results [19].

It should be noted that the maximal spreading diameter normalized by the droplet initial diameter scales differently with the Weber number and the Reynolds number in different regimes [8,15,34–38]. Since the analysis of flow focusing involves the droplet maximal spreading diameter, further studies are encouraged to explore whether the reported scalings of flow focusing time and the droplet jump-off force in this study are subject to change when a wider range of experimental parameters is investigated.

Although our experiments were conducted with impacting droplets, the physics in association with the jump-off force applies also to the coalescence-induced jumping droplets. The jump-off of an impacting droplet in this study and that of two coalescing droplets both stem from the horizontal-to-vertical redirection of the momentum. Specifically, the merging droplets in the horizonal direction squeeze, producing the vertically expanding liquid bridge that eventually hits the substrate and generates a droplet take-off [39].

D. The weakening of jump-off force for erosion protection

Since the droplet jump-off results from the flow focusing, a successful prediction of flow focusing time, droplet jump-off force, and jump-off pressure strongly corroborates our model. Considering the critical importance of flow focusing in determining the magnitude of the droplet jump-off force, from the practical perspective, weakening of the flow focusing is important to combat the substrate erosion shown in Fig. 1(a). The flow focusing can be hindered by breaking the symmetry and synchronicity of the retracting boundary, which can be achieved by fabricating a millimetric ridge with a height of 0.2 mm and a width of 0.1 mm on the substrate [40–42], as shown in the inset of Fig. 6(a). Indeed, the same experimental procedure as that in Fig. 2(b) results in a much

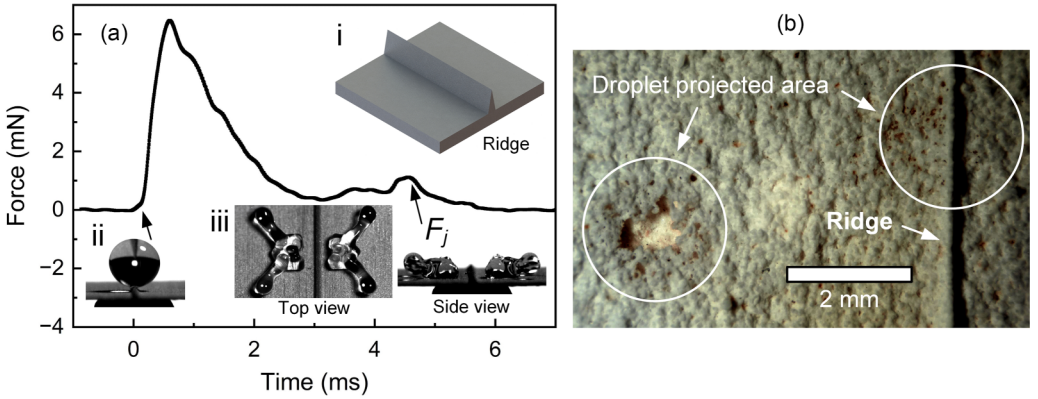

FIG. 6. (a) Temporal variation of the force exerted on a superhydrophobic substrate with a ridge height of 0.2 mm and a width of 0.1 mm shown in inset (i) caused by a 6.6-μl water droplet released at a height of 7 cm and the corresponding droplet shape profiles at various moments: (ii) the droplet just contacting the ridge; (iii) the top and side views of the droplet when the jump-off force is detected. (b) Surface morphology of a ridged (right) and plain [left, which is the same image in Fig. 1(a)] superhydrophobized plaster slab after being impacted by 6.6-μl water droplets released at a height of 5 cm at the rate of every 8 s for 4 h.

weaker jump-off force of ∼1.1 mN in Fig. 6(a) on the ridged superhydrophobic surface (see Video S2 in the Supplemental Material [28]) than that on its flat counterpart, ∼2.8 mN in Fig. 2(b). In addition, we allowed the water droplets to impact onto a ridged superhydrophobized plaster slab with a ridge height of 0.2 mm and a width of 0.1 mm using the same procedure adopted in the case shown in Fig. 1(a). No holes on the plaster slab were observed after a 4-h-long impact of water droplets, whereas a hole appeared after the location of the droplets' impact was moved from the ridge to a nearby flat area [Fig. 6(b)]. An in-depth investigation of droplet jump-off force on heterogeneous surfaces (e.g., ridged surfaces) will be conducted in the near future. This investigation will also include a systematic variation of the geometry of the surface microstructures [43,44], which represents an essential factor affecting the contact line dynamics of a droplet. This will enable us to incorporate the surface wetting characteristics into the evaluation of the jump-off force. The results of this investigation will be reported elsewhere.

IV. SUMMARY AND CONCLUSIONS

In summary, we have studied the origin and the dependence of the jump-off force imparted by a droplet to a superhydrophobic surface on various factors by systematically varying the droplet viscosity and the impact speed. We have supported the results from the literature claiming that the jump-off force scales linearly with the inertia-dominated impact force $\rho V_0^2 D_0^2$ using water droplets and found them to be invalid for droplets with different viscosities. We have introduced a timescale called flow focusing time and have measured it together with the droplet jump-off force using a high-resolution force sensing system. Based on the argument that the droplet jump-off results from momentum change in the vertical direction during flow focusing, models have been developed to predict the flow focusing time and the droplet jump-off force with an excellent agreement for droplets with varying viscosities. In contrast to the results reported in the literature, the jump-off force is determined synergistically by inertial, capillary, and viscous effects, and the scaling with $\rho V_0^2 D_0^2$ represents a special case when the viscous energy dissipation is negligible. We then demonstrated that the breaking of the symmetry and synchronicity of flow focusing can weaken the droplet jump-off force, which may have a great technological potential in applications such as erosion protection. An investigation of this phenomenon is now underway.

The authors declare no competing financial interest.

ACKNOWLEDGMENTS

The authors thank Jidong Gu for insightful comments in erosion protection. This work was partially supported by the Natural Science Foundation of China under Grant No. 12202108, Guangdong Basic and Applied Basic Research Foundation under Grants No. 2021A1515110184, No. 2022A1515011214, and No. 2021B0301030005, and by the GTIIT-Technion Seed Grant.

[1] C. Josserand and S. T. Thoroddsen, Drop impact on a solid surface, Annu. Rev. Fluid Mech. **48**, 365 (2016).
[2] A. L. Yarin, Drop impact dynamics: Splashing, spreading, receding, bouncing …, Annu. Rev. Fluid Mech. **38**, 159 (2005).
[3] X. Cheng, T.-P. Sun, and L. Gordillo, Drop impact dynamics: Impact force and stress distributions, Annu. Rev. Fluid Mech. **54**, 57 (2022).
[4] Y. Jiang, C. Machado, and K.-C. K. Park, From capture to transport: A review of engineered surfaces for fog collection, Droplet **2**, e55 (2023).
[5] C. Wei, Y. Zong, and Y. Jiang, Bioinspired wire-on-pillar magneto-responsive superhydrophobic arrays, ACS Appl. Mater. Interfaces **15**, 24989 (2023).
[6] Y. Zong, A. Oron, H. Liu, and Y. Jiang, Dynamic and quasi-static droplet penetration through meshes, Langmuir **39**, 9808 (2023).
[7] D. Richard, C. Clanet, and D. Quéré, Contact time of a bouncing drop, Nature (London) **417**, 811 (2002).
[8] C. Clanet, C. Béguin, D. Richard, and D. Quéré, Maximal deformation of an impacting drop, J. Fluid Mech. **517**, 199 (2004).
[9] B. Zhang, V. Sanjay, S. Shi, Y. Zhao, C. Lv, X.-Q. Feng, and D. Lohse, Impact forces of water drops falling on superhydrophobic surfaces, Phys. Rev. Lett. **129**, 104501 (2022).
[10] Q. Tang, S. Xiang, S. Lin, Y. Jin, C. Antonini, and L. Chen, Enhancing droplet rebound on superhydrophobic cones, Phys. Fluids **35**, 052101 (2023).
[11] V. Sanjay, P. Chantelot, and D. Lohse, When does an impacting drop stop bouncing?, J. Fluid Mech. **958**, A26 (2023).
[12] L. Gordillo, T.-P. Sun, and X. Cheng, Dynamics of drop impact on solid surfaces: Evolution of impact force and self-similar spreading, J. Fluid Mech. **840**, 190 (2018).
[13] B. Zhang, J. Li, P. Guo, and Q. Lv, Experimental studies on the effect of Reynolds and Weber numbers on the impact forces of low-speed droplets colliding with a solid surface, Exp. Fluids **58**, 125 (2017).
[14] D. Soto, A. B. De Larivière, X. Boutillon, C. Clanet, and D. Quéré, The force of impacting rain, Soft Matter **10**, 4929 (2014).
[15] Q.-P. Li, Y. Ouyang, X.-D. Niu, Y. Jiang, M.-F. Wen, Z.-Q. Li, M.-F. Chen, D.-C. Li, and H. Yamaguchi, Maximum spreading of impacting ferrofluid droplets under the effect of nonuniform magnetic field, Langmuir **38**, 2601 (2022).
[16] Z. Hu, F. Chu, and X. Wu, Double-peak characteristic of droplet impact force on superhydrophobic surfaces, Extreme Mech. Lett. **52**, 101665 (2022).
[17] B. Zhang, H. Zhao, Y. Zhao, P. Hao, and C. Lv, Impact force of ring bouncing on superhydrophobic surface with a bead, Phys. Fluids **35**, 052104 (2023).
[18] T.-P. Sun, F. Álvarez-Novoa, K. Andrade, P. Gutiérrez, L. Gordillo, and X. Cheng, Stress distribution and surface shock wave of drop impact, Nat. Commun. **13**, 1703 (2022).
[19] S. Ryu, P. Sen, Y. Nam, and C. Lee, Water penetration through a superhydrophobic mesh during a drop impact, Phys. Rev. Lett. **118**, 014501 (2017).
[20] M. A. Nearing, J. M. Bradford, and R. D. Holtz, Measurement of force vs. time relations for waterdrop impact, Soil Sci. Soc. Am. J **50**, 1532 (1986).
[21] M. Ahmad, M. Schatz, and M. V. Casey, Experimental investigation of droplet size influence on low pressure steam turbine blade erosion, Wear **303**, 83 (2013).

[22] T. Liu, J. Luo, Z. Zheng, T. Li, and S. He, Effects of rainfall intensity on splash erosion and its spatial distribution under maize canopy, Nat. Hazards **84**, 233 (2016).
[23] B. Amirzadeh, A. Louhghalam, M. Raessi, and M. Tootkaboni, A computational framework for the analysis of rain-induced erosion in wind turbine blades, part I: Stochastic rain texture model and drop impact simulations, J. Wind Eng. Ind. Aerodyn. **163**, 33 (2017).
[24] D. Bartolo, C. Josserand, and D. Bonn, Singular jets and bubbles in drop impact, Phys. Rev. Lett. **96**, 124501 (2006).
[25] S. Mitra, Q. Vo, and T. Tran, Bouncing-to-wetting transition of water droplets impacting soft solids, Soft Matter **17**, 5969 (2021).
[26] S. Lin, D. Wang, L. Zhang, Y. Jin, Z. Li, E. Bonaccurso, Z. You, X. Deng, and L. Chen, Macrodrop-impact-mediated fluid microdispensing, Adv. Sci. **8**, 2101331 (2021).
[27] J. Eggers, M. A. Fontelos, C. Josserand, and S. Zaleski, Drop dynamics after impact on a solid wall: Theory and simulations, Phys. Fluids **22**, 062101 (2010).
[28] See Supplemental Material at http://link.aps.org/supplemental/10.1103/PhysRevFluids.8.113601 for experimental procedures, experimental parameters, and supplemental videos for variation of the impact force and the corresponding droplet dynamics.
[29] Y. Jiang, C. Machado, S. Savarirayan, N. A. Patankar, and K.-C. Park, Onset time of fog collection, Soft Matter **15**, 6779 (2019).
[30] J. D. Paulsen, J. C. Burton, and S. R. Nagel, Viscous to inertial crossover in liquid drop coalescence, Phys. Rev. Lett. **106**, 114501 (2011).
[31] A. Jha, P. Chantelot, C. Clanet, and D. Quéré, Viscous bouncing, Soft Matter **16**, 7270 (2020).
[32] D. Bartolo, C. Josserand, and D. Bonn, Retraction dynamics of aqueous drops upon impact on non-wetting surfaces, J. Fluid Mech. **545**, 329 (2005).
[33] G. Taylor, The dynamics of thin sheets of fluid. III. Disintegration of fluid sheets, Proc. R. Soc. Lond. A **253**, 313 (1959).
[34] J. Madejski, Solidification of droplets on a cold surface, Int. J. Heat Mass Transf. **19**, 1009 (1976).
[35] E. W. Collings, A. J. Markworth, J. K. McCoy, and J. H. Saunders, Splat-quench solidification of freely falling liquid-metal drops by impact on a planar substrate, J. Mater. Sci. **25**, 3677 (1990).
[36] S. Chandra and C. T. Avedisian, On the collision of a droplet with a solid surface, Proc. R. Soc. Lond. A **432**, 13 (1991).
[37] M. Pasandideh-Fard, Y. M. Qiao, S. Chandra, and J. Mostaghimi, Capillary effects during droplet impact on a solid surface, Phys. Fluids **8**, 650 (1996).
[38] N. Laan, K. G. de Bruin, D. Bartolo, C. Josserand, and D. Bonn, Maximum diameter of impacting liquid droplets, Phys. Rev. Appl. **2**, 044018(R) (2014).
[39] T. Mouterde, T.-V. Nguyen, H. Takahashi, C. Clanet, I. Shimoyama, and D. Quéré, How merging droplets jump off a superhydrophobic surface: Measurements and model, Phys. Rev. Fluids **2**, 112001(R) (2017).
[40] A. Gauthier, S. Symon, C. Clanet, and D. Quéré, Water impacting on superhydrophobic macrotextures, Nat. Commun. **6**, 8001 (2015).
[41] Y. Liu, M. Andrew, J. Li, J. M. Yeomans, and Z. Wang, Symmetry breaking in drop bouncing on curved surfaces, Nat. Commun. **6**, 10034 (2015).
[42] M. Andrew, Y. Liu, and J. M. Yeomans, Variation of the contact time of droplets bouncing on cylindrical ridges with ridge size, Langmuir **33**, 7583 (2017).
[43] Y. Jiang, Y. Sun, J. W. Drelich, and C.-H. Choi, Topography-dependent effective contact line in droplet depinning, Phys. Rev. Lett. **125**, 184502 (2020).
[44] Y. Jiang and C.-H. Choi, Droplet retention on superhydrophobic surfaces: A critical review, Adv. Mater. Interfaces **8**, 2001205 (2021).